Thermally-Induced and Electron-Induced Chemistry of CF_3I on Ni(100)

M. B. Jensen and P. A. Thiel*

Contribution from the Department of Chemistry and Ames Laboratory, Iowa State University, Ames, Iowa 50011

Received July 18, 1994[⊗]

Abstract: We have investigated the thermally-induced and electron-impact-induced chemistry of CF_3I on Ni(100) following adsorption at 100 K. The data support a model for the thermally-induced chemistry, in which CF_3I dissociates to CF_3 and I, either upon adsorption or at slightly-elevated temperatures. Most CF_3 decomposes to adsorbed C and F. Above 75% saturation of the first layer, the availability of surface sites for decomposition decreases to a level where some adsorbed CF_3 remains intact and desorbs as such. Bombardment of multilayer CF_3I by low-energy electrons introduces new chemistry. Electron-induced decomposition (EID) of the parent molecule occurs through both C−I and C−F bond scission, with a measured cross section of 1.5×10^{-16} cm^2 (upper limit). Thermally-induced desorption from the electron-bombarded surface indicates a number of EID fragment reactions, most notably carbon−carbon bond formation, as evidenced by $C_2F_3I^+$, $C_2F_4^+$, $C_2F_5^+$, $C_3F_5^+$, and $C_4F_7^+$. To our knowledge, this is the first report of C−C bond formation in small fluorocarbons adsorbed on metal surfaces.

1. Introduction

The interaction of fluorocarbons with surfaces is fundamentally important in a wide variety of applications, from lubrication in the aerospace and magnetic media industries,[1,2] to fluorocarbon etching of electronic devices.[3−5] Furthermore, interactions of low-energy electrons with fluorocarbons are important in a number of surface-related processes. For instance, electron-impact events in fluorocarbon discharges lead to CF_x radical formation and, depending on the components of the discharge, eventual selective etching of Si or SiO_2.[5] Also, it has been reported that low-energy electrons or UV-induced photoelectrons cause increased adhesion of perfluoropolyether lubricants to several substrates through cross-linking of the polymer chains.[6] This has proven especially beneficial in computer disk lubrication, where lubricant−metal bonding is critical because of high disk rotation speeds.[2,7] Polymer chain cross-linking has also been reported after electron irradiation of polytetrafluoroethylene (Teflon).[8] This same effect has been noted for photon irradiation and is thought to be initiated by low-energy valence excitations resulting from secondary electrons.[9]

In spite of the importance of the topic, only one study to date has sought to clarify the interaction of low-energy electrons with small fluorocarbons adsorbed on a surface.[10] There, no evidence is reported for C−C bond formation (the fundamental step in cross-linking). The present paper deals with the electron-induced chemistry of CF_3I on Ni(100), establishing first the thermally-induced chemistry as a baseline. We find clear evidence for C−C coupling, but only after irradiation of the condensed multilayer. This may be a first step toward understanding cross-linking induced by electron bombardment of polymers.

2. Experimental Description

The experiments are performed in a previously described stainless steel vacuum chamber with a base pressure of 6×10^{-11} Torr.[11] Briefly, the chamber is equipped for Auger electron spectroscopy (AES), thermal desorption mass spectrometry (TDS), electron-stimulated desorption ion angular distribution (ESDIAD), low-energy electron diffraction (LEED), and gas introduction.

The disk-shaped Ni(100) single crystal, 1 mm thick and 9 mm in diameter, is spotwelded to two tapered tantalum rods for efficient resistive heating and is in thermal contact with a liquid nitrogen-coolable cold finger. Temperature is monitored with a W5%Re−W26%Re thermocouple spotwelded to the back of the crystal.

Initial cleaning of the freshly prepared Ni(100) single crystal is described elsewhere.[12] Major contaminants detected by AES are carbon, oxygen, and sulfur. Sulfur and oxygen are removed by argon ion bombardment, while small exposures of O_2 (0.3−0.7 L) followed by annealing at 1000 K serve to deplete the surface of residual carbon. Before each experiment the crystal is argon ion bombarded for 10−15 min to deplete the surface of sulfur and undesorbed iodine from CF_3I. This is followed by low exposures of O_2 at 300 K and 20−60 s anneals at 1000 K until the surface is clean, as determined by AES. AES peaks at 146 and 180 eV were originally attributed to residual sulfur and chlorine, respectively. Attempts to eliminate these peaks by excessive ion bombardment were unsuccessful. However, if the AES signal is collected at a crystal temperature of 900 K, these peaks disappear and are, therefore, determined to be electron diffraction peaks common to well-ordered Ni(100) surfaces.[13]

TDS experiments are performed using a UTI 100C quadrupole mass spectrometer (QMS) interfaced to a personal computer, thereby allowing simultaneous monitoring of up to eight masses. A feedback circuit in the design of Herz *et al.*[14] is used for control of the heating rate. For all TDS experiments, except where otherwise noted, the heating rate is 4 K/s to 250 K, and 2 K/s to 1200 K. Exposure is carried out at 100 K.

[⊗] Abstract published in *Advance ACS Abstracts,* December 1, 1994.

(1) Watson, N. D., et al., *NASA TM-87636*, 1985.
(2) Lee, H. J., et al. *J. Vac. Sci. Technol. A* **1993**, *11*, 711−714.
(3) Oehrlein, G. S.; Zhang, Y.; Vender, D.; Haverlag, M. *J. Vac. Sci. Technol. A* **1994**, *12*, 323−332.
(4) Oehrlein, G. S.; Zhang, Y.; Vender, D.; Joubert, O. *J. Vac. Sci. Technol. A* **1994**, *12*, 333−344.
(5) Robertson, R. M.; Golden, D. M.; Rossi, M. J. *J. Vac. Sci. Technol. B* **1988**, *6*, 1632−1640.
(6) Vurens, G. H.; Gudeman, C. S.; Lin, L. J.; Foster, J. S. *Langmuir* **1992**, *8*, 1165−1169.
(7) Lee, T.-H. D. *J. Vac. Sci. Technol. A* **1991**, *9*, 1287−1292.
(8) Rye, R. R. *J. Polym. Sci., Polym. Phys.* **1993**, *31*, 357−364.
(9) Rye, R. R.; Shinn, N. D. *Langmuir* **1990**, *6*, 142−146.
(10) Kiss, J.; Alberas, D. J.; White, J. M. *Surf. Sci.* **1992**, *275*, 82−91.
(11) Walczak, M. M.; Thiel, P. A. *Surf. Sci.* **1989**, *224*, 425−450.
(12) Wang, W.-D.; Wu, N. J.; Thiel, P. A. *J. Chem. Phys.* **1990**, *92*, 2025−2035.
(13) Becker, G. E.; Hagstrum, H. D. *J. Vac. Sci. Technol.* **1974**, *11*, 284−287.
(14) Herz, H.; Conrad, H.; Kuppers, J. *J. Phys. E* **1979**, *12*, 369.

0002-7863/95/1517-0438$09.00/0

In order to reduce stray electron current from the QMS ionizer to the crystal, three electrostatic lenses with 8 mm apertures separate the crystal from the ionizer. The lens closest to the ionizer is held at +5 V, while the middle lens is held at −55 V. The lens closest to the sample and the sample are grounded, with the distance from the crystal to the front of the ionizer being approximately 1.5 cm. In this configuration, stray electron current at the sample is reduced by 95%, from 2.8 μA to 100 nA.

The ionizer of the QMS is used as the electron source for studying the effects of low-energy electrons on the CF_3I chemistry. After dosing CF_3I, the sample is moved to the TDS position. The voltage bias is removed from the two electrostatic lenses closest to the ionizer, and a bias of +40 V is applied to the crystal. The ionizer emission current is 3.0 mA, resulting in a current from crystal to ground measured at approximately 6 mA. This current is used as an estimate of the electron flux incident on the crystal, although it is not corrected for secondary electron emission and is, therefore, a lower limit. The maximum incident electron energy is 110 eV.

CF_3I is purchased from PCR Inc., which specifies 99.0% purity. Several freeze−pump−thaw cycles are carried out under vacuum with liquid nitrogen for further purification. CF_3I is introduced into the chamber through a directional gas doser, consisting of a 2 mm diameter conductance-limiting aperture in series with a collimating aperture. The crystal is positioned approximately 0.5 cm from the doser end. Pressure in the doser line is 25−30 Torr, measured with a capacitance manometer. Exposures are reported in experimental units of Torr • seconds, or in relative units which give the percentage of the exposure required to saturate the decomposition products (notably iodine). Cracking of CF_3I in the QMS results in the following relative intensities: CF_3^+ (1.00), CF_3I^+ (0.89), I^+ (0.78), CF_2^+ (0.11), and CF^+ (0.08). These intensities are close to the standard reference fragmentation pattern of CF_3I^+ (1.00), I^+ (0.96), CF_3^+ (0.77), CF^+ (0.12), CF_2^+ (0.07).[15] We also establish the fragmentation pattern of CF_n species in situ by monitoring known CF_2 and CF_3 desorption states from CF_3I decomposition on Ru(001).[16] In this way, it is determined that the relative intensities of CF_3^+, CF_2^+, and CF^+ from CF_3 are 0.42, 1.00, and 0.45, respectively, while those of CF_2^+ and CF^+ from CF_2 are 1.00 and 0.86. These ratios differ from those reported previously by our laboratory,[16] because the QMS is retuned for the present experiments to maximize sensitivity for high masses (>40 amu).

3. Results

1. Thermal Chemistry of CF_3I on Ni(100). Figure 1 shows the yield of three main fragment ions, derived from three main desorbates, as a function of exposure. Evidence of C−I bond cleavage is given by the presence of an atomic iodine desorption state, represented by I^+ in Figure 1. Figure 2 shows the I^+ (m/z = 127) desorption traces with increasing CF_3I exposure. The peak temperature shifts from 1130 K at the lowest exposure to 1085 K at the highest exposure, indicative of adsorbate−adsorbate repulsive interactions and similar to atomic iodine desorption from Ru(001).[16] As shown in the top panel of Figure 1, the area under the I^+ curve grows monotonically with increasing exposure until reaching a saturation level at approximately 4000 Torr • s. Above this exposure, defined as 100% saturation-exposure, only the CF_3I multilayer state grows. At exposures approaching saturation and beyond, a small feature is seen in the I^+ signal at 885 K. We believe neither state of I^+ can originate from NiI_2 or IF, since no NiI^+ or IF^+ is detected.

Figure 3 shows the CF_3I^+ (m/z = 196) desorption traces at selected exposures. No sharp monolayer peak is evident. Instead, at 2000 Torr • s, or 50% saturation, a broad feature appears between 150 and 350 K. At 60% saturation this feature intensifies and gives the appearance of a doublet, one peak at 180 K, the other at approximately 270 K. Above this exposure

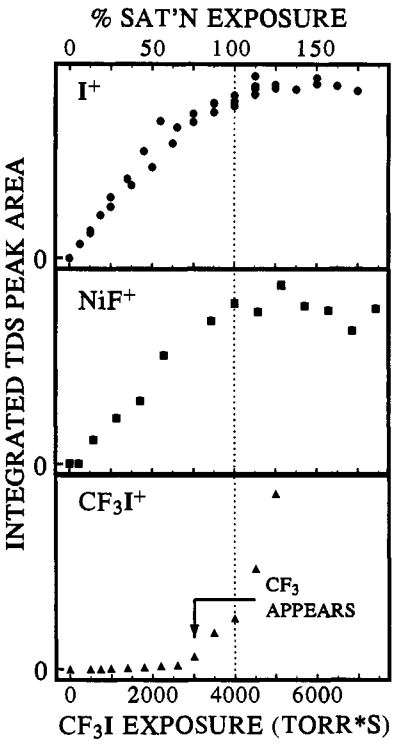

Figure 1. Integrated TDS peak area vs CF_3I exposure for CF_3I^+, NiF^+, and I^+. Saturation of C−I bond cleavage occurs at 4000 Torr • s. A CF_3 desorption state appears at 3000 Torr • s.

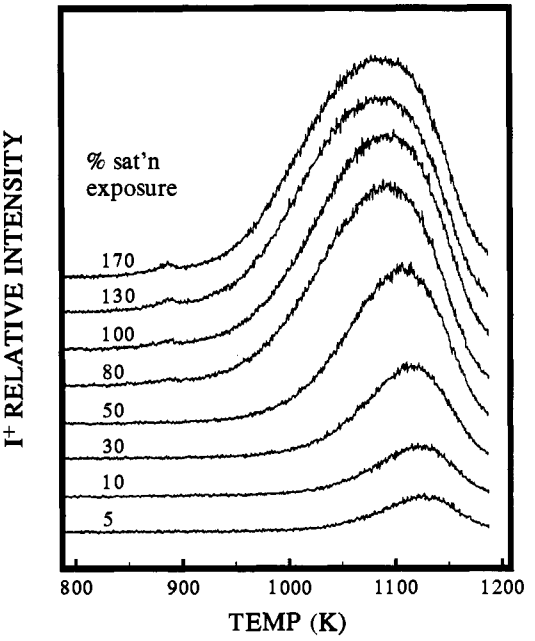

Figure 2. I^+ (m/z = 127) TDS signal for increasing exposures of CF_3I on Ni(100). A 4000 Torr • s exposure corresponds to saturation.

a sharp desorption state appears at 150 K and increases in intensity with all exposures thereafter, as shown in the inset of Figure 3 and in the bottom panel of Figure 1. This state is attributed to CF_3I multilayers. It should be noted that the broad feature between 150 and 350 K, although not visible because of the scale of the inset in Figure 3, remains as a high-temperature foot on the multilayer peak at all high exposures.

Carbon−fluorine bond scission is indicated by NiF_2 desorption at 885 K, concurrent with the low-temperature I^+ state. Ni^+, NiF^+, and NiF_2^+ are detected for all naturally occurring Ni isotopes, providing unambiguous determination of the parent

(15) Grasselli, J. G.; Ritchey, W. M., Eds. *CRC Atlas of Spectral Data and Physical Constants for Organic Compounds*; Chemical Rubber Company: Cleveland, 1975.

(16) Dyer, J. S.; Thiel, P. A. *Surf. Sci.* **1990**, *238*, 169−179.

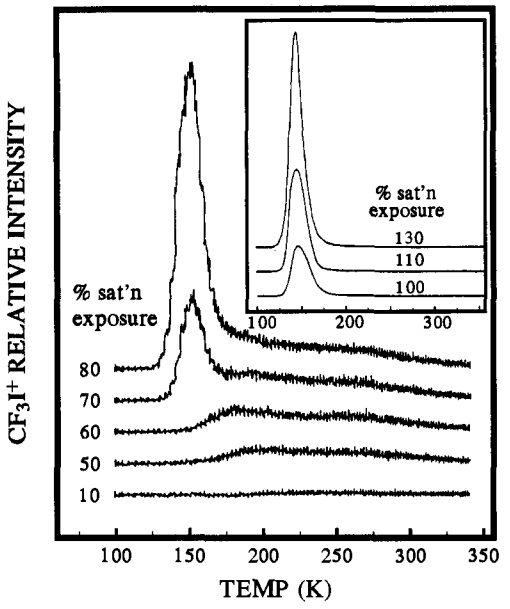

Figure 3. CF_3I^+ ($m/z = 196$) TDS signal for increasing exposures of CF_3I on Ni(100). The heating rate for exposures below saturation is 2 K/s, as opposed to the usual 4 K/s for this temperature range, in an attempt to resolve possible multiple molecular desorption states. For exposures at saturation and above, shown in the inset, the heating rate is 4 K/s.

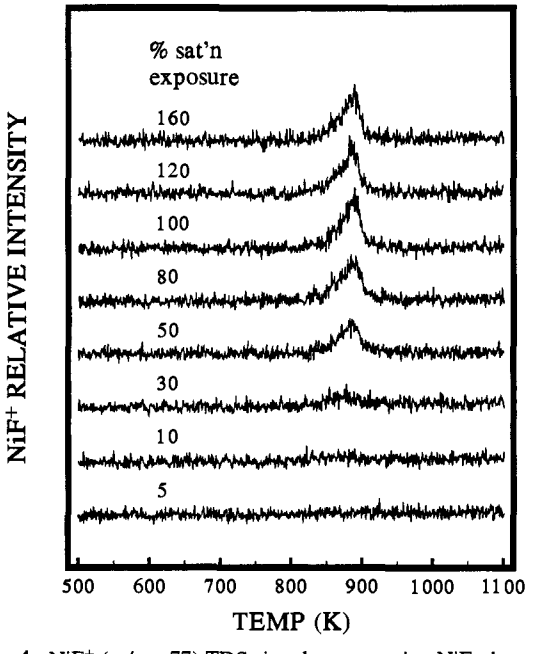

Figure 4. NiF^+ ($m/z = 77$) TDS signal, representing NiF_2 desorption, for increasing exposures of CF_3I on Ni(100) at 100 K.

species as NiF_2. Desorption traces of the strongest cracking fragment, $^{58}NiF^+$ ($m/z = 77$), are shown in Figure 4. There is no shift in the peak desorption temperature with increasing exposure. The middle panel of Figure 1 shows the NiF^+ desorption peak area vs CF_3I exposure. The NiF_2 state appears shortly after atomic iodine, and grows monotonically, saturating along with atomic iodine at 4000 Torr · s.

Figure 5 shows desorption traces in the temperature range 200−500 K for the major cracking fragments of CF_3I after a saturation exposure. At 340 K, a small peak exists in the CF_2^+ signal. Also at this temperature, a small rise above baseline is evident in the CF^+ signal. A small CF_3^+ peak may be discernible, but examination of similar data shows its existence

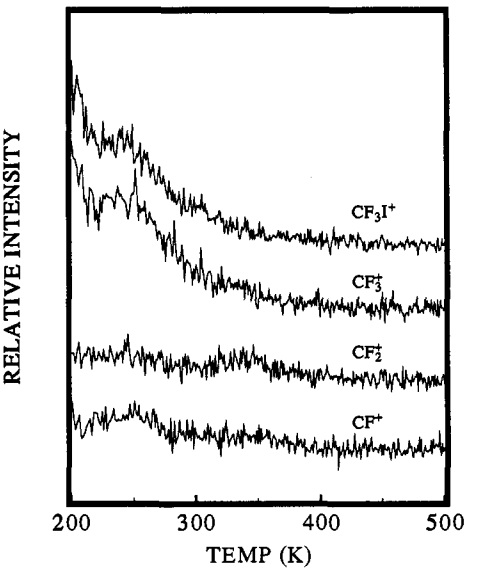

Figure 5. TDS spectra for CF_3I^+ ($m/z = 196$), CF_3^+ ($m/z = 69$), CF_2^+ ($m/z = 50$), and CF^+ ($m/z = 31$) for a saturation exposure, 4000 Torr · s, of CF_3I.

never to be obvious. Because the CF_2^+ signal for this state is approximately twice that of CF^+, and based on the cracking patterns established in Section 2, we attribute this state to a small amount of CF_3 desorption. This feature first appears at an exposure of approximately 75% saturation and is detected at all exposures thereafter, although always visible only slightly above the baseline.

The rapidly decreasing CF_3I^+ and CF_3^+ signals shown between 200 and 300 K in Figure 5 are interpreted as the high-temperature CF_3I foot coming off the large multilayer peak. Also in this temperature range, peaked at 250 K, a small CF^+ feature is visible, but too large to be due to QMS fragmentation of CF_3I. Since the absence of a corresponding CF_2^+ peak of similar height makes it impossible to attribute this state to CF_2 or CF_3I desorption (cf. Section 2), we believe it is due to a small amount of CF desorption. It is visible at all exposures equal to and above 90% saturation. We believe this small CF state originates from electron beam damage to CF_3I multilayers (cf. Section 3.2). Even though our electrostatic lens configuration limits the amount of stray electron current at the crystal, some current is still measured. If the ionizer of the QMS is left off until 200 K during TDS of a saturation exposure of CF_3I, this small CF^+ peak is not seen.

2. Electron-Induced Chemistry of CF_3I on Ni(100). As shown in Figure 6, CF_3I multilayers are very susceptible to EID. Figure 6 shows the CF_3I^+ ($m/z = 196$) TDS signal from a 5000 Torr · s CF_3I exposure after various low-energy ($E_i \leq 110$ eV) electron fluences at 100 K. The decreasing peak area indicates that CF_3I is consumed via EID.

The kinetic behavior of EID in multilayer CF_3I can be modeled as a first-order process,

$$-\mathrm{d}[CF_3I]/\mathrm{d}t = k[CF_3I] \quad (1)$$

where $[CF_3I]$ is the concentration of adsorbed CF_3I. The first-order rate constant, k, can be expressed:

$$k = (i_c/eA)\sigma_{EID} = \text{flux}\cdot\sigma_{EID} \quad (2)$$

where i_c is the current measured at the crystal, e is the electron charge, A is the surface area of the crystal, and σ_{EID} is the EID cross section. Equation 1 can then be solved to yield:

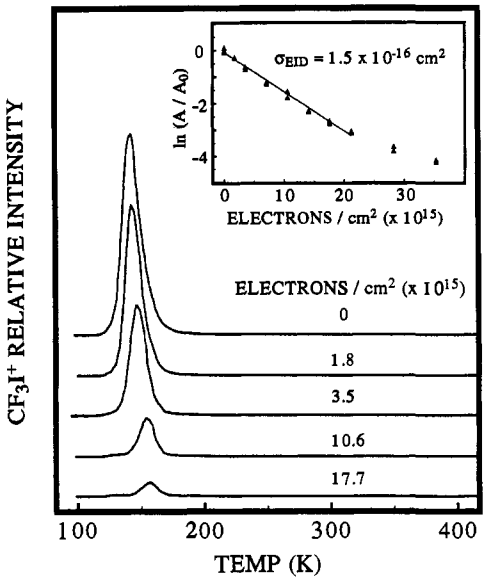

Figure 6. CF_3I^+ TDS signal from a 5000 Torr · s CF_3I exposure after increasing levels of electron fluence. Decreasing peak intensity indicates EID. The inset shows the linear relationship between $\ln(A/A_0)$ and electron fluence, resulting in $\sigma_{EID} = 1.5 \times 10^{-16}$ cm^2.

$$\ln(A_t/A_0) = -(i_c/eA)\sigma_{EID}t = -F_e\sigma_{EID} \qquad (3)$$

where F_e is the total electron fluence, A_t is the area under the TDS peak corresponding to t seconds of electron exposure, and $A_t/A_0 = [CF_3I]_t/[CF_3I]_0$. A plot of $\ln(A_t/A_0)$ vs F_e is shown in the inset of Figure 6. A slight deviation from linearity occurs at high electron fluences, probably due to inhibited EID from surface fragments—an effect reported previously for CF_3Cl on Pt(111).[10] From the plot in Figure 6, the cross section for EID, σ_{EID}, is calculated to be 1.5×10^{-16} cm^2. This value must be considered an upper limit since i_c is not completely corrected for secondary electron emission.

Products of electron-stimulated desorption (ESD) can be detected with the QMS during electron bombardment. The effects of a 2 min electron bombardment at 100 K on a 5000 Torr · s CF_3I exposure are shown in Figure 7. A bias of +40 V is applied to the crystal after 15 s to initiate the experiment. The species detected are F^+, HF^+, CF_n^+ ($n = 1-3$), I^+, and a small amount of CF_3I^+. HF^+ is probably the result of recombination in the QMS ionizer of fluorine from fluorinated ESD products and background H_2. Atomic fluorine is the dominant ESD product, which is not surprising, given the well-known susceptibility of fluorine to ESD.

A substantial amount of C−I bond scission results from electron bombardment. During irradiation, the QMS detects I^+, along with CF_n fragments. Most of the atomic iodine created as a result of electron-induced C−I bond scission is retained on the crystal surface. This is shown by TDS following electron bombardment; I^+ peak areas are plotted vs electron fluence in Figure 8. C−I bond scission occurs rapidly at first, leveling off after $20-25 \times 10^{15}$ electrons/cm^2. Upon electron irradiation, the small I^+ feature at 885 K intensifies along with the main I^+ state, while the NiF^+ feature at this same temperature remains constant (data not shown).

As reported below, we observe C−C bond formation products in post-EID TDS of CF_3I on Ni(100), yet we detect no $C_2F_3^+$ ($m/z = 81$), $C_2F_4^+$ ($m/z = 100$), $C_2F_5^+$ ($m/z = 119$), or $C_3F_5^+$ ($m/z = 131$) *during* electron bombardment.

A variety of decomposition products desorb during post-EID TDS. Figure 9 shows C_xF_yI desorption states from a 5000 Torr · s CF_3I exposure at increasing levels of electron fluence,

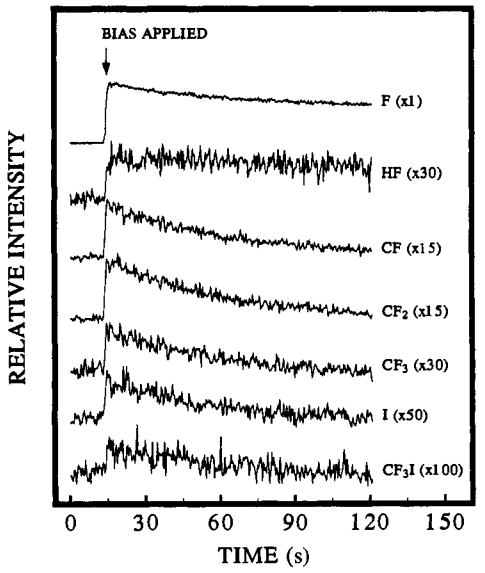

Figure 7. Species detected during EID after a 5000 Torr · s CF_3I exposure at 100 K. The electron flux is 5.89×10^{13} electrons s^{-1} cm^{-2}, and a 120 s dose corresponds to a fluence of 7.1×10^{15} electrons/cm^2.

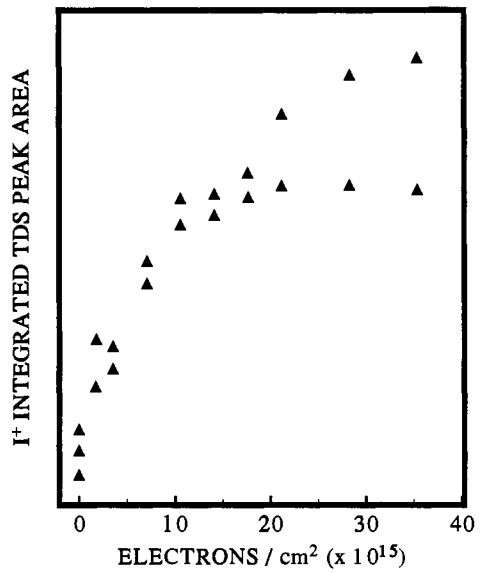

Figure 8. Integrated I^+ desorption peak area vs electron fluence for a 5000 Torr · s CF_3I exposure. The two curves represent two sets of experiments.

(i) to (vi). Two states can be seen in the CF_2I^+ ($m/z = 177$) spectrum of Figure 9A. The state at 150 K, overranged at low fluences, is due to molecular CF_3I, as shown previously in Figure 6. At 200 K, a second state emerges, initially increasing with electron fluence and then decreasing back to baseline level. No corresponding CF_3I^+ is visible. Therefore, we attribute this new desorption state to CF_2I, formed from CF_3I by electron-induced C−F bond cleavage. Finally, in data not shown, a small CFI state can be identified at 240 K, which appears and intensifies after the CF_2I state is in decline and then itself disappears. Thus, the three CF_nI species ($n = 3$, 2, 1) undergo sequential population and loss under the influence of the electron beam, as illustrated in Figure 10; note also the desorption at progressively higher temperatures (150, 200, 240 K).

A similar rise and fall, paralleling that of CF_2I, is seen in the $C_2F_3I^+$ ($m/z = 208$) signal at 180 K, shown in Figure 9B. Masses higher than 208 are not observed for this state. Candidate parent ions for this new species are C_2F_5I, C_2F_4I, and C_2F_3I. However, the known fragmention pattern

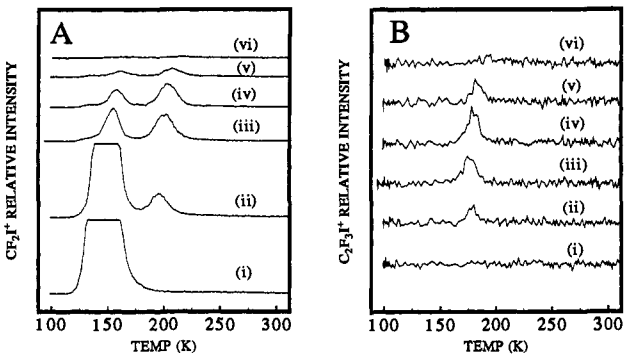

Figure 9. TDS signal for (A) CF_2I^+ and (B) $C_2F_3I^+$, after electron fluences of (i) 0, (ii) 3.5×10^{15}, (iii) 17.7×10^{15}, (iv) 24.7×10^{15}, (v) 35.3×10^{15}, and (vi) 70.7×10^{15} electrons/cm^2, after a 5000 Torr · s CF_3I exposure at 100 K.

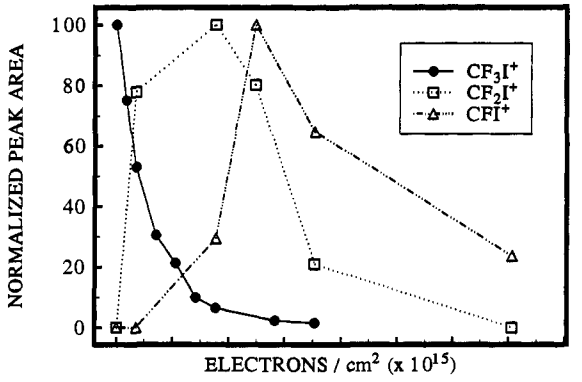

Figure 10. Yield of various species in TDS as a function of initial electron fluence at low temperature.

of C_2F_5I shows $C_2F_5I^+$ (m/z = 246) as the largest peak, with no perceptible $C_2F_3I^+$;[17] one would expect a similar pattern for C_2F_4I. Therefore, we can eliminate the first two species from consideration and attribute the state at 180 K to C_2F_3I. An independent measurement of the C_2F_3I cracking pattern[17] is consistent with this assignment. The formation of this product, as well as others (below), entails C−C bond formation.

Several new electron-induced features are also evident from the CF_n (n = 1−3) TDS results, shown in Figure 11 with increasing electron fluence. Sharp peaks at 150 and 200 K in the CF^+ spectrum of Figure 11A correspond to CF_3I and CF_2I, respectively, as described above. Consistent with this assignment, both peaks are evident in the CF_2^+ spectrum of Figure 11B, while the CF_3^+ spectrum of Figure 11C shows only the CF_3I state.

At 250 K, peaks arise in the CF^+ and CF_3^+ spectra. Assignment of this state to one desorbing species is difficult since no CF_2^+, and no higher masses, are detected at this temperature. In mass spectral cracking of CF_4(g), CF_3^+ is the main fragment, with no detectable CF_4^+, and very little CF_2^+ or CF^+.[15] As discussed in Section 2, if CF_2(g) were detected, CF_2^+ and CF^+ would be of roughly equal intensity. Therefore, we attribute the peaks at 250 K in the CF_3^+ and CF^+ spectra to reaction-limited CF_4 and CF.

A broad desorption state, centered at 350 K, can be seen in the CF^+ and CF_2^+ spectra. Since the two masses generate approximately equal signals at this temperature, we can attribute this state to CF_2 desorption. It is interesting to note that, as described above, in the absence of low-energy electrons, high exposures of CF_3I react on Ni(100) to give a CF_3 desorption state at this same temperature, 350 K.

(17) Jensen, M. B.; Thiel, P. A. Unpublished results.

Another broad state can be seen, this time in the CF_3^+ spectrum of Figure 11C. Its onset is at 340 K, peaking at 400 K and extending to 500 K. The state appears to be a superposition of two peaks, one peaked at 400 K and the other at 450 K. We attribute this state to products of electron-induced C−C bond formation. Figure 12 shows the major products detected in this same temperature range for a 5000 Torr · s CF_3I exposure bombarded by 17.7×10^{15} electrons/cm^2. CF_3^+ and $C_2F_4^+$ (m/z = 100) are the dominant species detected, followed by $C_3F_5^+$ (m/z = 131), $C_2F_5^+$ (m/z = 119), and $C_4F_7^+$ (m/z = 181). Also detected, but not shown, are small of amounts of $C_3F_6^+$ (m/z = 150) and $C_3F_3^+$ (m/z = 93). All species detected in this temperature range show the same peak shape and the same relative intensity response with respect to electron exposure. This response is shown in Figure 13, represented by $C_2F_4^+$. Initially, the state grows in intensity with increasing electron fluence, peaks at 17.7×10^{15} electrons/cm^2, and then decreases with higher electron fluence.

The parent ions corresponding to the state at 340−500 K are difficult to identify. We consider two main possibilities: only one species desorbs and we monitor a cracking pattern of that species, or a mixture of products evolves due to a series of reactions triggered by the same slow rate-determining step. In evaluating the first possibility, the relative intensities of the fragment species do not match the published mass spectral cracking patterns of any simple C_1−C_4 fluorocarbons.[15] From Figure 12, the fragmentation ratios are CF_3^+ (1.00), $C_2F_4^+$ (1.00), $C_3F_5^+$ (0.25), $C_2F_5^+$ (0.17), and $C_4F_7^+$ (0.12). It can be seen from Figure 11 that both CF^+ and CF_2^+ extend into this temperature range, but their relative contributions are difficult to estimate. The most intense fragments are CF_3^+ (m/z = 69) and $C_2F_4^+$ (m/z = 100). CF_3^+ is the main fragment in all C_1−C_6 noncyclic perfluoroalkanes, but $C_2F_4^+$ is much more rare. It appears as the strongest fragment of perfluorocyclobutane, which is, however, inconsistent with the rest of the fragments we observe.

We postulate, therefore, that a mixture of reaction-limited products desorb between 340 and 500 K (peak at 400 K). These products are the result of two or more reactions initiated by the same rate-determining step, which begins to occur at 340 K. Since we observe no desorption peak temperature shift in the C_n desorbing species, we assume this rate-limiting step is first order. A similar model has been proposed to explain the thermal chemistry of CH_3I on Cu(110).[18] There, evolution of a methane−ethylene mixture in a single first-order state is initiated by slow methyl decomposition to CH_2(ad) and H(ad).

We can use the fragmentation pattern to tentatively identify some of the products. All mass spectral cracking patterns are taken from the same reference.[15] The observation of $C_4F_7^+$ (m/z = 181) and $C_3F_5^+$ (m/z = 131) is especially helpful, as it indicates a perfluoroalkene, C_nF_{2n} (n = 3, 4), or a cyclic perfluoroalkane, C_nF_{2n} (n = 5, 6). A mixture of perfluoropropenes, namely 1-hexafluoropropene and 2-methyloctafluoropropene, can account best for the appearance and relative intensities of $C_4F_7^+$, $C_3F_6^+$, $C_3F_5^+$, and $C_3F_3^+$ that we observe, along with a portion of the CF_3^+. This leaves only $C_2F_4^+$, $C_2F_5^+$, and the remainder of the CF_3^+ fragments unexplained.

$C_2F_4^+$ may arise from C_2F_5 radical desorption. Mass spectrometric detection of the C_2F_5 radical, with electron-impact ionization, has been accomplished by monitoring $C_2F_5^+$ (m/z = 119).[19] However, we have been unable to obtain an entire mass spectral fragmentation pattern of this radical. It is not

(18) Chiang, C.-M.; Wentzlaff, T. H.; Bent, B. E. *J. Phys. Chem.* **1992**, *96*, 1836−1848.

(19) Butkovskaya, N. I.; Larichev, M. N.; Leipunskii, I. O.; Morozov, I. I.; Tal'roze, V. L. *Dokl. Phys. Chem.* **1978**, *240*, 442−443.

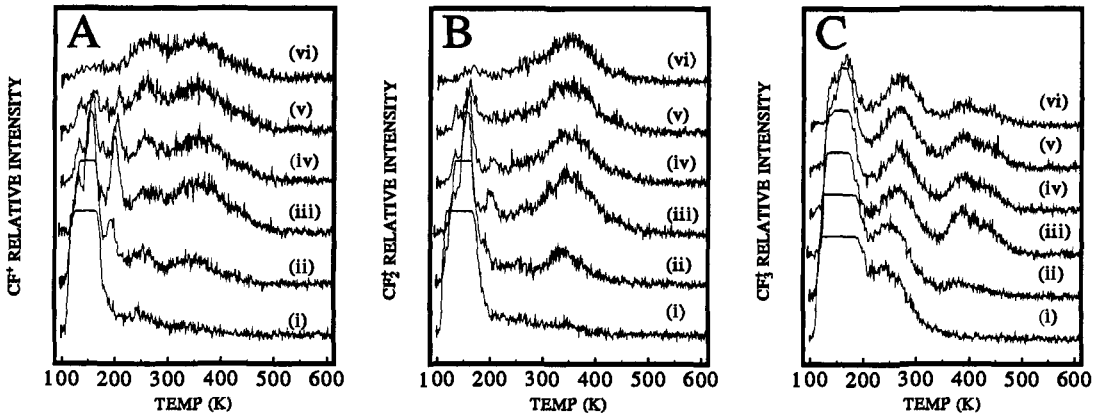

Figure 11. TDS signal for (A) CF^+, (B) CF_2^+, and (C) CF_3^+ after electron fluences of (i) 0, (ii) 3.5×10^{15}, (iii) 17.7×10^{15}, (iv) 24.7×10^{15}, (v) 35.3×10^{15}, and (vi) 70.7×10^{15} electrons/cm^2, after a 5000 Torr · s CF_3I exposure.

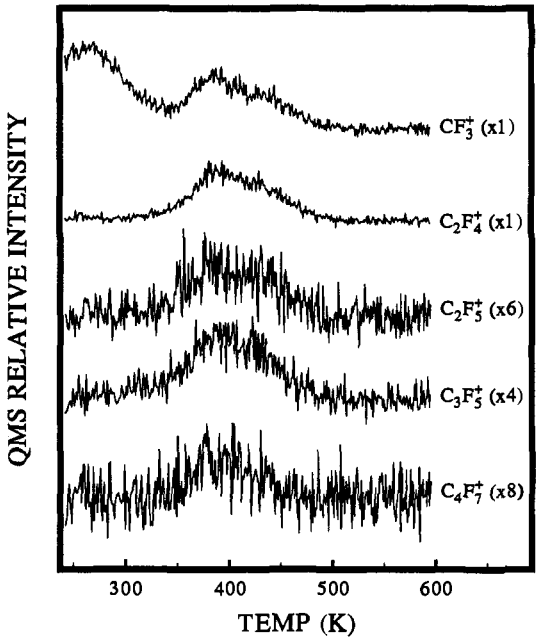

Figure 12. Species with C−C bonds detected after 5000 Torr · s CF_3I exposure, plus EID, at 100 K. The electron fluence is 17.7×10^{15} electrons/cm^2.

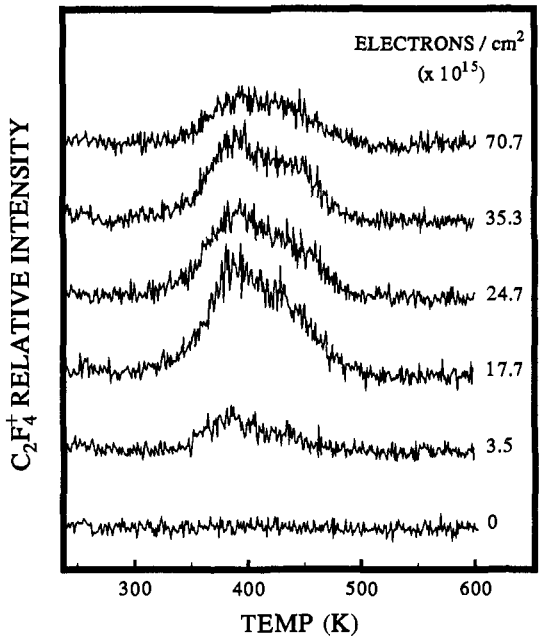

Figure 13. Response of the $C_2F_4^+$ TDS signal to increasing electron fluences. The CF_3I exposure is 5000 Torr · s in each case.

difficult to imagine that the major fragment will result from the loss of one fluorine atom, as has been observed for the CF_3 radical.[16] We note also the thermodynamic stability of the C_2F_5 radical ($H_f = -217.3$ kcal/mol).[20]

The remainder of the large CF_3^+ signal, as well as a portion of the $C_2F_5^+$ signal, can be attributed to a saturated fluorocarbon, most probably C_2F_6. CF_3^+ is generally the largest fragment in saturated fluorocarbons, e.g. more than twice the size of the next largest, $C_2F_5^+$, in C_2F_6. We can, therefore, postulate that the series of C−C bond formation products desorbing between 350 and 500 K result from rate-determining C_2F_5(ad) activation, followed by formation and desorption of $CF_3CF{=}CF_2$, $CF_3C(CF_3){=}CF_2$, and C_2F_6.

4. Discussion

1. Thermal Chemistry of CF_3I on Ni(100). The thermal chemistry of CF_3I on Ni(100) is summed up by the peak area vs exposure plots shown in Figure 1 for the major desorbing species. Atomic iodine desorption begins at lowest exposure, followed by NiF_2 at 600 Torr · s; both grow monotonically to saturation at 4000 Torr · s. At 75% saturation, 3000 Torr · s, the small CF_3 desorption state appears. Molecular CF_3I rises slowly between 50 and 75% and then grows rapidly with the appearance of the multilayer. It is interesting to note that the multilayer state appears below saturation exposure, indicating multilayer island population before the completion of C−I bond cleavage.

We do not observe a sharp CF_3I peak for a chemisorbed layer, as has been seen for other metals;[16,21,22] instead, there is a very broad molecular CF_3I desorption state between 150 and 300 K. Given the persistence of this state to relatively high temperatures, we speculate that this small feature is due to recombination of adsorbed CF_3 and I, with the CF_3 possibly stabilized by defect sites or slight impurities. Following vacuum breaks, we detect high levels of sulfur contamination and notice a large amount of CF_3 desorption at 350 K after CF_3I exposure, indicating that impurities can stabilize adsorbed CF_3 against dissociation.

Based on the TDS data, a simple model can be developed for the reactions of monolayer CF_3I on Ni(100). CF_3I dissociates to CF_3 and I, either upon adsorption or at slightly-elevated

(20) Weast, R. C., Ed. *CRC Handbook of Chemistry and Physics*; Chemical Rubber Company: Cleveland, 1986−87.

(21) Castro, M. E., et al. *J. Phys. Chem.* **1993**, *97*, 8476−8484.

(22) Liu, Z.-M.; Zhou, X.-L.; Kiss, J.; White, J. M. *Surf. Sci.* **1993**, *286*, 233−245.

temperatures. In a reaction which probably occurs through impurity- or defect-oriented channels, a small amount of CF_3 recombines with I below 300 K to desorb as CF_3I. (Note that the breadth of this peak suggests unusual recombination kinetics, such as kinetic parameters which vary with coverage or binding site.) However, most CF_3 decomposes to adsorbed C and F. (Although there is a slight difference in the exposures at which I(g) and NiF_2(g) first appear, we can assume that they are both formed at the lowest exposures; it has been documented that low vapor pressure solids, such as NiF_2, are difficult to detect by mass spectrometry due to their high sticking coefficient on chamber surfaces.[18]) At exposures above 75% saturation, the availability of surface sites for decomposition decreases to a level where some adsorbed CF_3 remains intact and desorbs as such. Except for the defect- or impurity-mediated recombination, this model is very similar to that proposed for CH_3I on Ni(100).[23-26]

In our data, the concurrence of NiF_2 and I desorption at 885 K suggests another type of reaction. The I^+ state appears only near saturation and is very small relative to the main I^+ state at higher temperature. One possible explanation is that adsorbed F and I segregate into separate islands. As coverage reaches saturation, these island boundaries begin to interact. Therefore, when NiF_2 desorbs, the local disruption of the Ni lattice causes desorption of adjacent I. Limiting the reaction to island boundaries accounts for the small size of the I^+ feature at 885 K. While EID produces a higher concentration of I(ad), the NiF_2 concentration remains constant as EID-induced atomic fluorine is ejected into the gas phase. Hence, more I(ad) interacts with the same amount of NiF_2. This is consistent with the increase in the I^+ yield at 885 K resulting from electron bombardment, as well as the unchanged NiF_2 yield.

A comparison of the thermal chemistry of CF_3I, CH_3I,[23-26] and C_2H_5I[27] on Ni(100) indicates that this surface is very effective in activating both C−F and C−H bonds of the simple halocarbons. Ag(111) lies at the other extreme, with no evidence of either C−F or C−H bond cleavage in the simple halocarbons.[21,28] Other metal surfaces, however, are more discriminatory between C−F and C−H bonds. For instance, the reactivity of Ru(001) toward CF_3I is intermediate between that of Ni(100) and Ag(111),[16] whereas Ru(001) is even more active than Ni(100) for CH_3 decomposition.[28,29]

2. Electron-Induced Chemistry of CF_3I on Ni(100). Efficient EID of multilayer CF_3I occurs on Ni(100) with a cross section, σ_{EID}, of 1.5×10^{-16} cm^2. We observe two types of products from this process: gaseous species which evolve during electron bombardment; and products which remain at the surface, reacting and/or desorbing during subsequent heating. The main component of the former group is atomic fluorine; lesser amounts of CF_n ($n = 1-3$), I, and CF_3I are also detected. No products of C−C bond formation are in this group. Interestingly, C_2H_5(g) and C_2H_6(g) are detected during EID of adsorbed CH_3Cl on Ag(111).[30]

Post-irradiation TDS shows a number of new products. While molecular CF_3I decreases in intensity, a CF_2I state grows in at 200 K and then disappears with increasing electron fluence; as it disappears, a CFI state develops at 240 K and again disappears. This sequence, illustrated in Figure 10, is evidence that electron-induced decomposition proceeds in a stepwise fashion:

$$CF_3I \rightarrow CF_2I + F \rightarrow CFI + 2F$$

The fluorine liberated in this reaction may contribute to that which is observed in the gas phase during EID. The increase in desorption temperature corresponding to loss of fluorine indicates that as C−F bonds break, the surface−molecule interaction intensifies. A similar sequential defluorination has been observed in EID of PF_3 on Ru(001).[31]

A number of CF_n products are also observed. CF and CF_4 are detected simultaneously at 250 K, while CF_2 is seen at 350 K. The relatively high temperature for CF_4 desorption indicates a reaction-limited process. Since CF desorption occurs simultaneously, we can imagine a disproportionation reaction of the sort:

$$CF_3(ad) + CF_2(ad) \rightarrow CF_4(g) + CF(g)$$

The greater abundance and variety of CF_n species observed in post-EID TDS, relative to normal TDS, may result from a site-blocking effect: EID produces an abundance of fragments at low temperature, which are then stable because the sites needed for thermally-induced decomposition are occupied. Thus, electron impact inhibits subsequent thermal dissociation at the metal surface.

In EID of CF_3Cl on Pt(111),[10] decomposition occurs with a probability close to ours, $\sigma_{EID} = 7 \times 10^{-16}$ cm^2. However, in the CF_3Cl work, no C−C bond formation products are reported, either during electron irradiation or in post-irradiation TDS. The difference may stem from the fact that our work focusses on *multilayer* CF_3I, while the CF_3Cl/Pt(111) study focusses on *monolayer (chemisorbed)* CF_3Cl. Several other studies have shown that electron-induced coupling occurs readily in hydrocarbons on metal surfaces.[30,32-36] The mechanism is generally thought to be initiated by electron-induced bond dissociation, followed by coupling of the remaining fragments.[30] More specifically for this discussion, perfluorinated molecules are especially susceptible to dissociative electron attachment, resulting in a F^- ion and a radical. This process has, in fact, been suggested as the initiation step in the cross-linking of perfluoropolyethers.[6] It is reasonable to expect that a proximate metal surface might shorten the lifetime, either of the initial ionized molecule (via quenching) or of the resultant free radical, and that electron-induced chemistry would thus be more effective farther from the metal, i.e. more effective in a multilayer than in a monolayer. Comparing the CF_3Cl/Pt(111) work with ours suggests that this is the case, although a more systematic comparison would strengthen that conclusion. Finally, this scenario suggests that electron-induced chemistry in multilayers, not monolayers, is most relevant to that in bulk polymers.

For our system, we postulate the following picture. Incident electrons create fluorocarbon radicals from randomly-oriented,

(23) Zhou, X.-L.; White, J. M. *Surf. Sci.* **1988**, *194*, 438−456.
(24) Zhou, X.-L.; White, J. M. *Chem. Phys. Lett.* **1987**, *142*, 376−380.
(25) Tjandra, S.; Zaera, F. *Langmuir* **1992**, *8*, 2090−2097.
(26) Tjandra, S.; Zaera, F. *J. Vac. Sci. Technol. A* **1992**, *10*, 404−405.
(27) Tjandra, S.; Zaera, F. *Surf. Sci.* **1993**, *289*, 255−266.
(28) Zhou, X.-L.; Solymosi, F.; Blass, P. M.; Cannon, K. C.; White, J. M. *Surf. Sci.* **1989**, *219*, 294−316.
(29) Zhou, X.-L.; Yoon, C.; White, J. M. *Surf. Sci.* **1988**, *206*, 379−394.
(30) Zhou, X.-L.; Blass, P. M.; Koel, B. E.; White, J. M. *Surf. Sci.* **1992**, *271*, 427−451.
(31) Madey, T. E., et al. In *Desorption Induced by Electronic Transitions DIET V*; Burns, A. R., Stechel, E. B., Jennison, D. R., Eds.; Springer-Verlag: Berlin, 1992; Vol. 31, p 182.
(32) Zhou, X.-L.; Blass, P. M.; Koel, B. E.; White, J. M. *Surf. Sci.* **1992**, *271*, 452−467.
(33) Zhou, X.-L.; Castro, M. E.; White, J. M. *Surf. Sci.* **1990**, *238*, 215−225.
(34) Castro, M. E.; Pressley, L. A.; White, J. M. *Surf. Sci.* **1991**, *256*, 227−241.
(35) Zhou, X.-L.; White, J. M. *J. Phys. Chem.* **1992**, *96*, 7703−7708.
(36) Zhou, X.-L.; White, J. M. *J. Chem. Phys.* **1990**, *92*, 5612−5621.

physisorbed molecules; these radicals are then free to desorb, and/or to react further. Some fragments react within the multilayer, whereas others reach the metal surface before reacting/desorbing. Some single-carbon fragments are created. Some of these appear in post-EID TDS as CF_2I and CFI (200, 240 K), while others remain at the metal to higher temperature. Those retained at the metal give rise to the CF and CF_4 desorption states at 250 K, as well as the CF_2 state peaked at 350 K. Two-carbon fragments also form, leading to C_2F_3I in post-EID TDS. Some C_2 fragments are also retained at the metal surface in the form of C_2F_5. These chemisorbed C_2 fragments are activated in the temperature range 340−500 K, yielding a mixture of C_2F_5(g), C_3F_6(g), C_4F_8(g), and C_2F_6(g). It is not clear from our data exactly which reactions occur in the multilayer and which in the monolayer, although it seems probable that the iodine-containing fragments form in the multilayer, given the effectiveness of the Ni(100) surface for C−I bond breaking in the absence of electrons. Hence, the observation of the two-carbon iodide, C_2F_3I, suggests significant C−C bond formation within the multilayer.

5. Summary

The following model for the reactions of CF_3I on Ni(100) develops from our data. The thermally-induced chemistry is simple. Adsorption at 100 K is followed by C−I bond cleavage, either upon adsorption or in the initial stages of heating, resulting in CF_3(ad) and I(ad). CF_3(ad) readily decomposes to C(ad) and F(ad) at low coverages. At coverages approaching saturation of the first layer, CF_3 decomposition is suppressed by lack of surface sites, and a small CF_3 desorption state appears. F(ad) desorbs as NiF_2 at 885 K, accompanied by a small amount of atomic iodine at exposures approaching saturation, while the main iodine state is observed at 1130−1085 K. A CF_3I multilayer state is seen at 150 K, even before the decomposition products are saturated.

The electron-induced chemistry is complex. Irradiation of multilayer CF_3I with low-energy electrons ($E_i \leq 110$ eV) causes EID with a cross section, σ_{EID}, of 1.5×10^{-16} cm^2. Atomic fluorine is the dominant gaseous product observed during irradiation. Atomic iodine, produced by electron-induced C−I bond scission, is retained at the surface, as evidenced by an increase in the I^+ integrated TDS peak area with electron fluence. Post-irradiation TDS identifies a number of unique electron-induced reaction products. Sequential defluorination of CF_3I yields CF_2I and CFI. CF_2 is another new desorption product, and there is some evidence that adsorbed CF_2 reacts with CF_3, to yield other new gaseous products: CF_4 and CF. A group of fragment ions containing C−C bonds also are detected in a single desorption peak; the parent ions may be CF_3CF_2(g), $CF_3CF{=}CF_2$(g), $CF_3C(CF_3){=}CF_2$(g), and a saturated perfluorocarbon, probably C_2F_6(g). These could all form upon rate-limiting activation of CF_3CF_2(ad), a possible product of electron irradiation. Carbon−carbon bond formation is also evident in detection of an iodine-containing molecule, C_2F_3I.

Acknowledgment. Thanks are due to R. Rye and D. Saperstein for originally bringing the electron- and photon-induced chemistry of fluoropolymers to our attention and to C. Jenks and W. Trahanovsky for insightful discussions of halocarbon chemistry. This work is supported by the Ames Laboratory, which is operated for the U.S. Department of Energy by Iowa State University under contract No. W-7405-Eng-82. In addition, the work is supported by a GAANN Fellowship from the Department of Education (M.B.J.).

JA942340O